Optics Communications 542 (2023) 129596

Contents lists available at ScienceDirect

Optics Communications

journal homepage: www.elsevier.com/locate/optcom

Comparison of post-equalizers for beyond 100-Gb/s/λ C-band signal transmission over a 100-km dispersion-uncompensated SSMF

Xiong Wu [a,b], Junwei Zhang [a,b,*], Alan Pak Tao Lau [c,b], Chao Lu [a,b]

[a] Photonics Research Institute, Department of Electronic and Information Engineering, The Hong Kong Polytechnic University, Hong Kong Special Administrative Region of China

[b] The Hong Kong Polytechnic University Shenzhen Research Institute, Shenzhen, China

[c] Photonics Research Institute, Department of Electrical Engineering, Hong Kong Special Administrative Region of China

ARTICLE INFO

Keywords:
Intensity modulation and direct detection (IM/DD)
Nonlinear equalizer (NLE)
Absolute-term
Weight sharing

ABSTRACT

A comprehensive comparison among different post-equalizers with relatively low complexity is studied for C-band 100-km dispersion-uncompensated standard single-mode fiber (SSMF) intensity modulation and direct detection (IM/DD) transmission systems with data rate beyond 100 Gb/s/λ. These representative post-equalizers include feed-forward equalizer (FFE), polynomial-based nonlinear FFE (P-NFFE), absolute-term based nonlinear FFE (AT-NFFE), FFE combined with decision-feedback equalizer (FFE-DFE), polynomial based nonlinear FFE-DFE (P-NLE), absolute-term based nonlinear FFE-DFE (AT-NLE), and their lower-complexity versions of FFE-DFE-WS, P-NLE-WS, and AT-NLE-WS which use weight sharing (WS) to eliminate weight redundancy. We demonstrate 100-Gb/s/λ and 112-Gb/s/λ on-off keying (OOK) transmissions over a 100-km SSMF. For 112-Gb/s transmission, BERs of FFE-DFE(-WS), P-NLE(-WS), and AT-NLE(-WS) can reach 7% hard-decision forward error correction (HD-FEC) limit at 3.8×10^{-3}. Under 7% HD-FEC limit, AT-NLE-WS with 32 real-valued multiplications shows similar BER performance as P-NLE and AT-NLE with a small power penalty of < 0.4 dB, but outperforms P-NLE-WS, AT-NLE, and P-NLE in huge complexity reduction of approximately 83.2%, 92.4%, and 92.7%, respectively. Therefore, taking both the BER performance and the operation complexity into account, AT-NLE-WS is the optimal equalizer and is a strong candidate to be applied in low-cost C-band IM/DD interconnections with data rates beyond 100 Gb/s/λ and transmission distance up to 100 km.

1. Introduction

Required by the ever-increasing Internet traffic in data center interconnections (DCIs), high-speed fiber-optic communication systems at a transmission distance of up to 100 km are pursued in a cost-effective manner, especially in C-band transmission. Recently, several quasi-coherent/self-coherent solutions [1–6] have been proposed and verified for re-constructing the complex field of in-phase and quadrature (I/Q) modulation. These schemes simplify the receiver structure and reduce the cost from the conventional coherent receiver and detection, using fewer optical components, optoelectronic components, and analog-to-digital converters (DACs). However, these systems still require complicated algorithms, especially algorithms for polarization demultiplexing if dual-polarization signals are transmitted, and pose high implementation complexity. Furthermore, some phase retrieval solutions, using dispersion diversity and/or space diversity [7–10], have also been experimentally demonstrated for retrieving the phase of I/Q signals from direct detection (DD). But they rely on complex iterative algorithms and require many photodetectors (PDs) and dispersive media.

Although the cost, footprint, and power consumption of the commercial high-speed coherent applications or the simple high-speed quasi-coherent realization are being reduced in DCIs [11–13], efforts on strengthening high-speed IM/DD systems to extend the transmission distance have also been made recently [14–17]. The potential of robust IM/DD compensation/equalization algorithms should be further exploited in high-speed transmissions with distances reaching tens to hundreds of kilometers, signaling on-off-keying (OOK) or four-level pulse amplitude modulation (PAM-4). However, the existing fiber chromatic dispersion (CD) in dispersion-uncompensated standard single-mode fiber (SSMF) transmission becomes a major concern to high-speed IM/DD systems, especially in C-band transmission. Different equalization algorithms and their combination have been extensively explored to combat the large CD-induced frequency power fading. These include: linear and nonlinear Tomlinson–Harashima precoding (THP)

* Corresponding author at: Photonics Research Institute, Department of Electronic and Information Engineering, The Hong Kong Polytechnic University, Hong Kong Special Administrative Region of China.

E-mail address: jun-wei.zhang@polyu.edu.hk (J. Zhang).

https://doi.org/10.1016/j.optcom.2023.129596
Received 21 December 2022; Received in revised form 18 March 2023; Accepted 11 May 2023
Available online 18 May 2023

Table 1
Previous single-wavelength ≥50-Gb/s and ≥100-km IM/DD demonstrations.

References	DSP	Rate	Distance	FEC
Goeger, 2016 [44]	Tx: Phase retrieval Rx: DD-FFE	56 Gb/s (OOK)	110 km	7% HD-FEC
Rath et al. 2017 [18]	Tx: THP Rx: FFE	56 Gb/s (PAM-4)	100 km	20% SD-FEC
Zhou et al. 2020 [34]	Rx: PNLE+MLSE	56 Gb/s (OOK)	100 km	9% SD-FEC
Wang et al. 2020 [35]	Rx: PNLE+FFE-DFE+MLSE	64 Gb/s (OOK)	100 km	7% HD-FEC
Zhu et al. 2021 [14]	Rx: VDFE	80 Gb/s (OOK)	100 km	20% SD-FEC
Zhang et al. 2021 [39]	Rx: TCNN	56 Gb/s (PAM-4)	100 km	7% HD-FEC
Wu et al. 2022 [29]	Rx: AT-NLE-WS, *etc*.	85 Gb/s (OOK)	100 km	5.8% KP4-FEC
Li et al. 2022 [15]	Tx: THP Rx: FFE	56 Gb/s (PAM-4)	120 km	20% SD-FEC
Hu et al. 2022 [16]	Rx: Hybrid MCIA	112 Gb/s (PAM-4)	100 km	7% HD-FEC
Wu et al. 2022 [17]	Tx: Pre-distortion + pulse shaping Rx: AT-NLE-WS	120 Gb/s (PAM-4)	100 km	7% HD-FEC
This work	**Rx: AT-NLE-WS, *etc*.**	100 Gb/s (OOK) 112 Gb/s (OOK)	100 km	5.8% KP4-FEC 7% HD-FEC

DD-FFE: decision-directed feed-forward equalizer; PNLE: polynomial nonlinear equalizer; MLSE: maximum likelihood sequence estimation; VDFE: simplified Volterra-FFE-Volterra-DFE; TCNN: nonlinear equalizer based on temporal convolutional neural network regression model; AT-NLE-WS: absolute-term based nonlinear FFE-DFE with weight sharing; Hybrid MCIA: hybrid Gerchberg–Saxton multi-constraint iterative algorithm combining with linear equalization.

schemes at the transmitter side [15,18–20]; nonlinear feed-forward equalizers (NFFEs) at the receiver side [19,21–27]; FFE combined with decision-feedback equalizer (FFE-DFE) [18,28,29], its improved variants [30,31], and its nonlinear versions using absolute terms [29,32], polynomial [29,32–35], and Volterra series [14], at the receiver side; pre-compensation together with the nonlinear equalizers [17]; maximum likelihood sequence estimation (MLSE) and its simplified variants at the receiver side [34–36]; machine learning schemes at the transmitter side and/or at the receiver side [37–41]. Besides, some iterative algorithms for CD compensation have been experimentally proposed, including transmitter-side ones [42,43] and receiver-side phase retrieval algorithms [16,44,45]. These algorithms are based on the Gerchberg–Saxton algorithm [46], using a pair of forward-propagation and back-propagation along dispersive digital SSMF with certain constraints in an iterative manner. Moreover, some phase retrieval schemes require extra pilot symbols to decrease the phase error in iterative procedures. Nevertheless, the Volterra series based schemes, MLSE schemes, machine learning schemes, and iterative schemes all pose huge computational complexity when achieving a better performance.

For the reader's convenience, different IM/DD equalization schemes are summarized and listed in Table 1, which are recently verified in OOK or PAM-4 demonstrations with rates >50 Gb/s and distance of 100 km and above. More details can be found in the corresponding references.

Among these techniques in Table 1, post-equalizers pose a relatively low complexity and achieve comparable performance simultaneously. Even though they have been widely studied to combat CD-induced impairments in high-speed transmissions, their comparison, in terms of computational complexity and equalization performance, has not been fully investigated, especially with a distance reaching 100 km. Hence, in this paper, a comprehensive comparison of commonly-used post-equalizers is conducted for C-band OOK signal transmissions over a 100-km dispersion-uncompensated SSMF with single-wavelength data rates up to 100 Gb/s and 112 Gb/s. Besides applying the absolute operation to avoid multiplication operation [23,25,26,29,32], weight-sharing based on the *k*-means clustering algorithm [29,47,48] is also introduced in absolute-term based nonlinear FFE-DFE with weight sharing (AT-NLE-WS), which consequently reduce the weight redundancy and operational complexity. To show the superiorities in equalization performance and computational complexity of the AT-NLE-WS, a systematic investigation of the 100-km OOK transmission systems based on various post-equalizers, including FFE, polynomial-based nonlinear FFE (P-NFFE), absolute-term based NFFE (AT-NFFE), FFE-DFE, polynomial based nonlinear FFE-DFE (P-NLE), AT-NLE, and FFE-DFE-WS, P-NLE-WS, and AT-NLE-WS, are carried out in the context of parameter optimization, evaluation of the required number of real-valued multiplications per symbol (RNRM), and bit error rate (BER) measurements. The experimental results indicate that in both 100-Gb/s and 112-Gb/s OOK transmission systems over a 100-km SSMF, the BERs of all FFEs cannot reach 7% hard-decision forward error correction (HD-FEC) limit of 3.8×10^{-3} due to suffering severe frequency power fading, while the BER of the FFE-DFE cannot approach the KP4-FEC limit of 2.4×10^{-4} in 100-Gb/s case. With respect to NLEs under KP4-FEC (7% HD-FEC) limit, the 28-cluster (32-cluster) AT-NLE-WS with 28 (32) real-valued multiplications reduces the RNRM of approximately 84.3%, 92.6%, and 93.6% (83.2%, 92.4%, and 92.7%) compared with P-NLE-WS, AT-NLE, and P-NLE, respectively, in 100-Gb/s (112-Gb/s) OOK transmission over a 100-km SSMF. These show the superiorities of AT-NLE-WS in low-cost C-band IM/DD interconnections with data rate beyond 100 Gb/s/λ and transmission distance up to 100 km.

The remainder of this paper is organized as follows. Section 2 illustrates the principles and RNRMs of the abovementioned post-equalizers. Section 3 presents the experimental setup and the analysis of the experimental results of 100-Gb/s/λ OOK and 112-Gb/s/λ OOK transmissions over a 100-km SSMF. Section 4 draws the conclusion.

2. Principles and computational complexity of the performed post-equalizers

2.1. FFE and FFE-DFE

In IM/DD systems, FFE is a popular and robust linear finite impulse response (FIR) equalizer for compensating linear inter-symbol interference (ISI). However, it is limited in compensation for the spectral notches caused by CD-induced frequency power fading, even with a long memory length. To simultaneously compensate both the precursor ISI and CD-induced frequency power fading, the best choice for equalization is the combination of a FFE and a DFE called FFE-DFE, in which the DFE with an infinite impulse response (IIR) structure can effectively equalize the spectral notches by pole insertion [18,31,49,50]. The equalized output of FFE-DFE can be given by:

$$y(n) = \underbrace{\sum_{k=0}^{N_1-1} h_1(k)x(n-k)}_{\text{FFE}} + \underbrace{\sum_{k=1}^{D_1} l_1(k)d(n-k)}_{\text{DFE}}, \tag{1}$$

where $x(n-k)$ and $d(n-k)$ are the linear input term and hard decision term, respectively; $h_1(k)$ and $l_1(k)$ are the corresponding linear weights of N_1-tap FFE and D_1-tap DFE, respectively, which are estimated via the training sequence using the recursive least square (RLS) algorithm [51,52] in this paper. Note that we choose RLS algorithm instead of the least mean squares (LMS) algorithm in the training phase for fast convergence. Obviously, $y(n)$ turns to be the equalized output of FFE when $D_1 = 0$. Consequently, the RNRMs of FFE and FFE-DFE are N_1 and $N_1 + D_1$, respectively.

2.2. Second-order P-NFFE and P-NLE

In addition to linear ISI and CD-induced frequency power fading, the modulation- and transceiver-related nonlinearities arisen from the electrical amplifiers, modulators, and PD should also be considered. Therefore, the second-order polynomial nonlinear terms can be introduced in the FFE-DFE, which is then called second-order P-NFFE-DFE (P-NLE for short) and can be applied and expressed as [21,24,29,32,33]:

$$\begin{aligned} y(n) = & \underbrace{\sum_{k=0}^{N_1-1} h_1(k)\,x(n-k) + \sum_{k=0}^{N_2-1} h_2(k)\,x^2(n-k)}_{\text{P-NFFE}} \\ & + \underbrace{\sum_{k=1}^{D_1} l_1(k)d(n-k)}_{\text{DFE}}, \end{aligned} \tag{2}$$

where $x^2(n-k)$ and $h_2(k)$ are the second-order nonlinear term and the corresponding weight, respectively. Thus the RNRMs of P-NFFE and P-NLE are $N_1 + 2N_2$ and $N_1 + 2N_2 + D_1$, respectively.

2.3. AT-NFFE and AT-NLE

To reduce the equalization complexity of P-NFFE and P-NLE, we replace the second-order terms with absolute terms consuming less computational complexity, which are called AT-NFFE and AT-NFFE-DFE (AT-NLE for short), respectively. The absolute terms can be expanded using Taylor series, with the combinations of second-order and higher-order terms, in which the second-order terms are dominant [25,26,32]. Furthermore, the absolute-term-based nonlinear equalizers have been proposed and verified in our previous works [26,29,32] and as well in other works [23,25]. The equalized output of the AT-NLE is given by [29,32]:

$$\begin{aligned} y(n) = & \underbrace{\sum_{k=0}^{N_1-1} h_1(k)\,x(n-k) + \sum_{k=0}^{N_{AT}-1} h_{AT}(k)\,|x(n-k)|}_{\text{AT-NFFE}} \\ & + \underbrace{\sum_{k=1}^{D_1} l_1(k)d(n-k)}_{\text{DFE}}, \end{aligned} \tag{3}$$

where $|x(n-k)|$ and $h_{\text{AT}}(k)$ are the absolute term and its corresponding weight, respectively. It is seen that the multiplication operation for the calculation of $x^2(n-k)$ is completely avoided. Hence, the RNRMs of AT-NFFE and AT-NLE are $N_1 + N_{AT}$ and $N_1 + N_{AT} + D_1$, respectively.

2.4. FFE-DFE-WS, P-NLE-WS, and AT-NLE-WS

In [29], we proposed the AT-NLE-WS which is based on k-means clustering algorithm for weight sharing/clustering. With weight sharing/clustering in the training phase, the redundancy in weights can be reduced, naturally resulting in a significant reduction of computational complexity in the following equalization phase.

We first define:

$$\mathbf{h}(n) = [\boldsymbol{\alpha}, \boldsymbol{\beta}]^T, \tag{4}$$

where $[\cdot]^T$ stands for the transposition; $\boldsymbol{\alpha} = \left[h_1(0), \ldots, h_1\left(N_1-1\right), h_{AT}(0), \ldots, h_{AT}\left(N_{AT}-1\right)\right]^T$, $\boldsymbol{\beta} = \left[l_1(1), \ldots, l_1\left(D_1\right)\right]^T$.

$$\mathbf{s} = [\mathbf{x}, \mathbf{d}]^T, \tag{5}$$

where $\mathbf{x} = \left[x(n), \ldots, x\left(n-N_1+1\right), |x(n)|, \ldots, |x\left(n-N_{AT}+1\right)|\right]^T$, $\mathbf{d} = \left[d(n-1), \ldots, d\left(n-D_1\right)\right]^T$.

Then we rewrite the AT-NLE in Eq. (3) as:

$$y(n) = \mathbf{h}^T\mathbf{s}, \tag{6}$$

By applying the k-means clustering algorithm, the weights in $\mathbf{h}$ with similar values are clustered into one centroid $w((i)$ and then the equalized output of the AT-NLE-WS can be expressed as:

$$y(n) = \sum_{i=1}^{N_c} w(i)\,x_c(n,i), \tag{7}$$

where $w(i)$, N_c, and $x_c(n,i)$ are the centroid (namely the weight of AT-NLE-WS), the number of clusters, and the summation of the corresponding terms in $\mathbf{s}$ whose weights in $\mathbf{h}$ belong to the same cluster $w(i)$. Similar expressions for FFE-DFE-WS and P-NLE-WS can be deduced in the same manner, which are omitted here for simplicity.

In summary, the process of weight estimation using the RLS algorithm [51,52] and weight sharing using the k-means clustering algorithm [29,47,48] for the weight-shared equalizers of FFE-DFE-WS, P-NLE-WS, and AT-NLE-WS is as follows:

(1) Weight vector $\mathbf{h}$ is estimated for FFE-DFE ($N_1 + D_1$ weights), P-NLE ($N_1 + N_2 + D_1$ weights), or AT-NLE ($N_1 + N_{AT} + D_1$ weights) using RLS algorithm via the training symbols.
(2) N_c centroids are initially chosen from all the estimated weights in $\mathbf{h}$.
(3) For each weight in $\mathbf{h}$, the Euclidean distance is calculated between it and each centroid $w(i)$. Then it is assigned to the nearest cluster.
(4) The centroids are updated by calculating the mean of each cluster.
(5) Steps (3) and (4) are repeated until the standard metric function converges.
(6) The final N_c-centroid $\mathbf{w} = \left[w(1), \ldots, w\left(N_c\right)\right]^T$ is obtained for equalization.

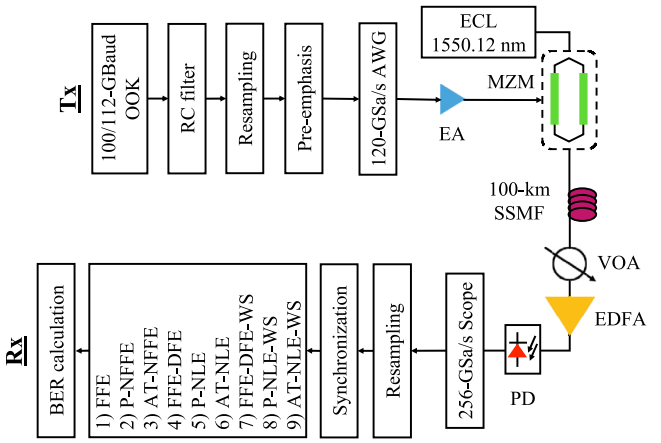

Fig. 1. Experimental setup of 100-km SSMF system with 100-GBaud/112-GBaud OOK transmission.

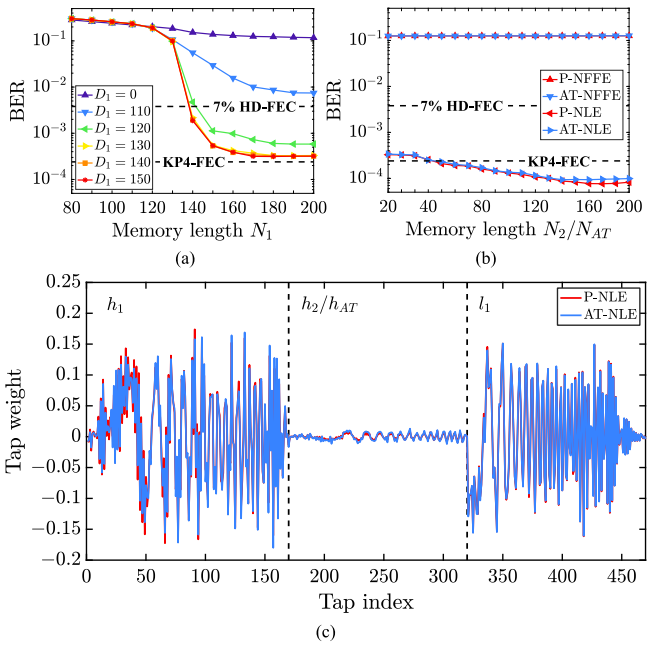

Fig. 2. (a) BER versus memory length of N_1 for FFE under different D_1 for DFE; (b) BER versus memory length of N_2/N_{AT} for FFE of P-NFFE/AT-NFFE (N_1 = 170 and D_1 = 0) and P-NLE/AT-NLE (N_1 = 170 and D_1 = 150); (c) tap weight distribution of 170-tap h_1, 150-tap h_2/h_{AT}, and 150-tap l_1 for P-NLE/AT-NLE, at a ROP of −12.8 dBm for 100-GBaud OOK transmission over a 100-km SSMF.

Therefore, compared with FFE-DFE and AT-NLE, the RNRMs of N_c-centroid FFE-DFE-WS and AT-NLE-WS are reduced from $N_1 + D_1$ to N_c and $N_1 + N_{AT} + D_1$ to N_c, respectively. The RNRM of N_c-centroid P-NLE-WS is $N_c + N_2$ with requiring additional N_2 real-valued multiplications for second-order polynomial terms. Since the IM/DD fiber channel is quasi-invariant, the training process is not necessary once the weight coefficients of the equalizers are estimated. Therefore, we mainly consider the computational complexity of equalization process for the equalizers.

3. Experimental setup and results

Fig. 1 illustrates the experimental setup of our 100-km SSMF system with 100-GBaud/112-GBaud OOK transmission. OOK signal is digitally raise-cosine (RC) pulse shaped with a roll-off factor of 0.1 and resampled to 120-GSa/s sampling rate. Then pre-emphasis is performed to mitigate the bandwidth limitation of the back-to-back (B2B) link. Next, digital-to-analog conversion is performed for the OOK signal via the arbitrary waveform generator (AWG, *Keysight* M8194A, ∼45-GHz 3-dB bandwidth) operating at a sampling rate of 120 GSa/s. Amplified by an electrical amplifier (EA, *SHF* S807, 50-GHz 3-dB bandwidth), the OOK signal drives the chirp-free Mach–Zehnder modulator (MZM, *Fujitsu* FTM7938EZ, ∼32-GHz 3-dB bandwidth) biased at the quadrature point, to realize the linear IM at 1550.12 nm with an external cavity laser (ECL). After transmitted through a 100-km SSMF, the distorted OOK signal sequentially goes through an optical variable attenuator (VOA) for varying the received optical power (ROP), an erbium-doped fiber amplifier (EDFA) for outputting the constant power, followed by a ∼70-GHz PD for realizing DD. Then the detected waveform is digitalized by an oscilloscope (OSC, *Keysight* UXR0804A, ∼80-GHz 3-dB bandwidth) operating at a sampling rate of 256 GSa/s, and digitally processed offline with a series of DSP procedures, including resampling to 2 samples per symbol, synchronization, equalization with different post-equalization algorithms, and BER calculation. These algorithms include: (1) FFE; (2) P-NFFE; (3) AT-NFFE; (4) FFE-DFE; (5) P-NLE; (6) AT-NLE; (7) FFE-DFE-WS; (8) P-NLE-WS; (9) AT-NLE-WS. The weights of all equalizers are estimated via the 10,000 prior-to-signal training symbols, using the RLS algorithm. Note that the BER is evaluated by 15 data frames, each containing 10,000 training symbols and 121,072 data symbols, 2^{17} symbols in total.

3.1. 100-GBaud OOK results

First, the performance of 100-GBaud OOK signal is evaluated after 100-km SSMF transmission. Under the maximal ROP of −12.8 dBm, the memory lengths of N_1, N_2/N_{AT}, and D_1 are determined from the BER results shown in Fig. 2. In Fig. 2(a) for FFE-DFE, it is observed that the BER performance gets better with larger N_1 and D_1. With only FFE performed ($D_1 = 0$), the BER is hard to be lower than 1×10^{-1}, as the purple curve with the filled up-triangles shows in Fig. 2(a). With the help of DFE ($D_1 \geq 110$) to mitigate the CD-induced frequency power fading, the BER is considerably decreased and is lower than 7% HD-FEC BER limit of 3.8×10^{-3}. Besides, the saturated BER of $\sim 3 \times 10^{-3}$ is achieved with N_1 of 170 and D_1 of 150, which is lower than the 7% HD-FEC BER limit but is slightly larger than the KP4-FEC BER limit of 2.4×10^{-4}.

To reach the KP4-FEC limit, nonlinear equalization should be considered. Implemented with $N_1 = 170$ and $D_1 = 150$, the impact of nonlinear memory length N_2/N_{AT} on BER performance for P-NLE and AT-NLE are then evaluated and the results are shown in Fig. 2(b). The saturated BERs for P-NLE and AT-NLE are achieved with the same nonlinear memory length of 150 at a BER of $\sim 1 \times 10^{-4}$, already lower than the KP4-FEC limit. Besides, the impact of N_2/N_{AT} on the BER performance for P-NFFE (P-NLE with $D_1 = 0$) and AT-NFFE (AT-NLE with $D_1 = 0$) can also be obtained from the results, which are marked as red up-triangles and blue down-triangles, respectively, in Fig. 2(b). Under the proposed 100-GBaud OOK transmission over a 100-km SSMF, the P-NFFE and AT-NFFE have the trivial improvement in the BER performance compared with FFE [purple up-triangles in Fig. 2(a)]. Fig. 2(c) illustrates the weight distributions of 170-tap h_1, 150-tap h_2, and 150-tap l_1 P-NLE and 170-tap h_1, 150-tap h_{AT}, and 150-tap l_1 AT-NLE. It reveals that the weights of P-NLE and AT-NLE are close. Although the weights of second-order and absolute terms are much smaller than those of linear and decision terms, they are essential to reduce the BER from $\sim 3 \times 10^{-4}$ to $\sim 1 \times 10^{-4}$. Fig. 3 presents the BER as a function of the number of training symbols of 100-GBaud OOK signal transmission over a 100-km SSMF using FFE-DFE, P-NLE, and AT-NLE with the optimized memory lengths. One can see that 10,000 training symbols that we adopt in all experiments are enough for the three equalizers to achieve the saturated BERs, namely convergence.

Furthermore, the electrical spectrum of the received signal after 100-km SSMF transmission is presented in Fig. 4, along with the spectra

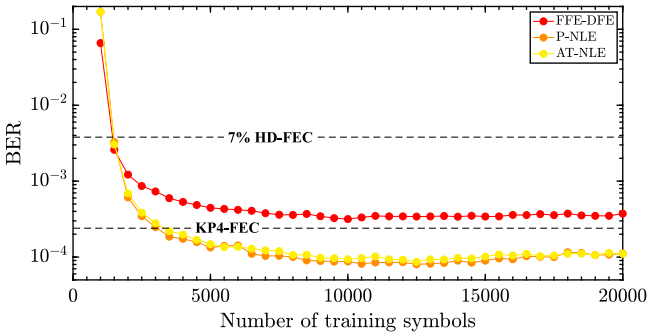

Fig. 3. BER versus the number of training symbols of 100-GBaud OOK signal transmission over a 100-km SSMF using different equalizers.

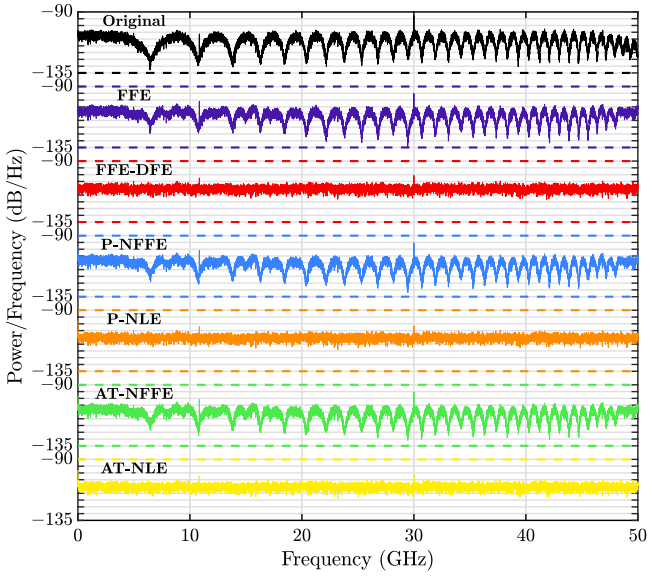

Fig. 4. Electrical spectra of the received 100-GBaud OOK signal after 100-km SSMF transmission, and the compensated signals with FFE, FFE-DFE, P-NFFE, P-NLE, AT-NFFE, and AT-NLE, respectively.

of the recovered signal using the abovementioned FFE ($N_1 = 170$), P-NFFE ($N_1 = 170$ and $N_2 = 150$), AT-NFFE ($N_1 = 170$ and $N_{AT} = 150$), FFE-DFE ($N_1 = 170$ and $D_1 = 150$), P-NLE ($N_1 = 170$, $N_2 = 150$, and $D_1 = 150$), and AT-NLE ($N_1 = 170$, $N_{AT} = 150$, and $D_1 = 150$). Apparently, there are still frequency notches in electrical spectra after equalization by the FFE, P-NFFE, and AT-NFFE. Thanks to the DFE for compensating the CD-induced frequency power fading, the FFE-DFE, P-NLE, and AT-NLE all can eliminate the frequency notches, beneficial to the decrease of BER.

Taking the values of $N_1 = 170$ and $D_1 = 150$ for FFE-DFE, $N_1 = 170$, $N_2 = 150$, and $D_1 = 150$ for P-NLE, and $N_1 = 170$, $N_{AT} = 150$, and $D_1 = 150$ for AT-NLE, the estimated weights of them are clustered for the weight-shared FFE-DFE-WS, P-NLE-WS, and AT-NLE-WS, respectively, using *k*-means clustering algorithm. The results of these equalizers with weight sharing are evaluated under different preset number of clusters as depicted in Fig. 5. Increasing the number of clusters, the BER performance for FFE-DFE-WS, P-NLE-WS, or AT-NLE-WS is first improved. Subsequently, the BER performance of FFE-DFE-WS, P-NLE-WS, and AT-NLE-WS is saturated at the number of clusters of approximately 54, requiring much fewer weights and achieving similar BERs as FFE-DFE, P-NLE, and AT-NLE, respectively. Moreover, the weight distribution of 54-cluster AT-NLE-WS along with AT-NLE's is shown in Fig. 5(b) for comparison. It is seen that the weights of AT-NLE with similar values are clustered together as the new one [hollow circles marked

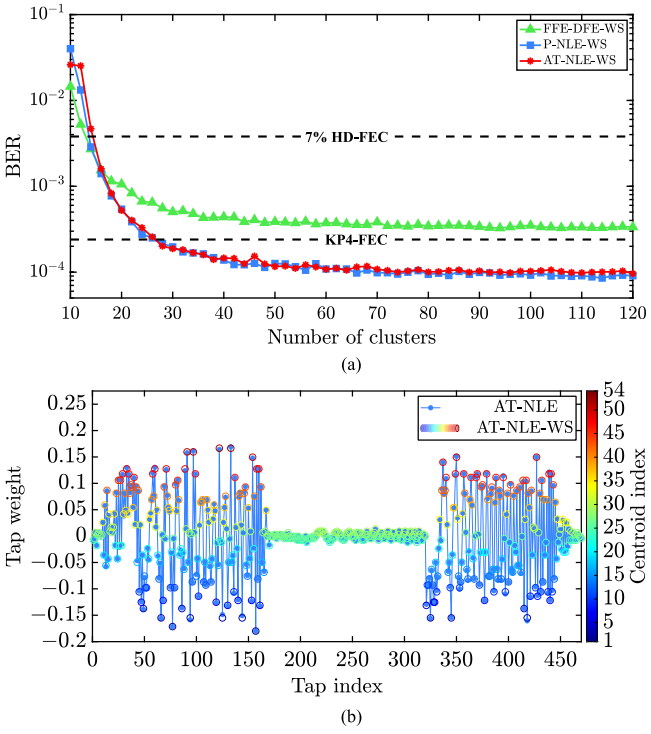

Fig. 5. (a) BER versus the number of clusters for FFE-DFE-WS, P-NLE-WS, and AT-NLE-WS; (b) tap and centroid weight distributions of 54-cluster AT-NLE-WS and 170-tap h_1, 150-tap h_{AT}, and 150-tap l_1 for AT-NLE, respectively, at a ROP of −12.8 dBm for 100-GBaud OOK transmission over a 100-km SSMF.

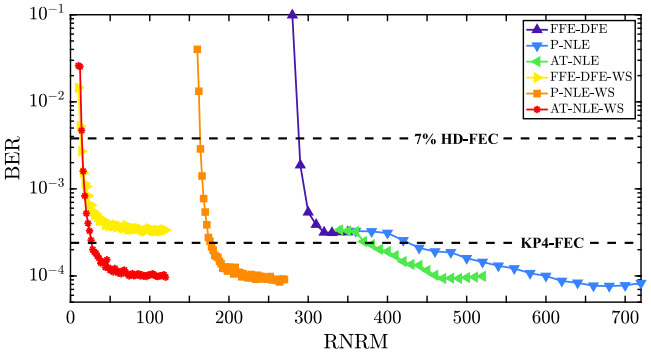

Fig. 6. BER versus RNRM using FFE-DFE, P-NLE, AT-NLE, FFE-DFE-WS, P-NLE- WS, and AT-NLE-WS at a ROP of −12.8 dBm for 100-GBaud OOK transmission over a 100-km SSMF.

in the same color] for equalization in AT-NLE-WS, thus reducing the computational complexity.

The BER as a function of RNRM of the abovementioned six equalizers, calculated according to complexity analysis in Section 2, are presented in Fig. 6. In detail:

- For FFE-DFE, the RNRM is changed from 280 to 350 by varying the N_1 from 130 to 200, with fixing D_1 at 150;
- For P-NLE, the RNRM is changed from 340 to 720 by varying the N_2 from 20 to 200, with fixing N_1 at 170 and D_1 at 150;
- For AT-NLE, the RNRM is changed from 280 to 350 by varying the N_{AT} from 20 to 200, with fixing N_1 at 170 and D_1 at 150;
- For FFE-DFE-WS, the RNRM is changed from 10 to 120 by varying the N_c from 10 to 120, clustering the estimated 320 weights from FFE-DFE with $N_1 = 170$ and $D_1 = 150$;

Table 2
Key RNRMs [in Fig. 6] of all equalizers for 100-Gb/s OOK transmission over a 100-km SSMF.

Equalizer	RNRM at 3.8 × 10–3	RNRM at 2.4 × 10–4	RNRM at saturated BER
FFE-DFE	≥290	\	320
P-NLE	≥360	≥440	620
AT-NLE	≥340	≥380	470
FFE-DFE-WS	≥14	\	54
P-NLE-WS	≥164	≥178	204
AT-NLE-WS	≥16	≥28	54

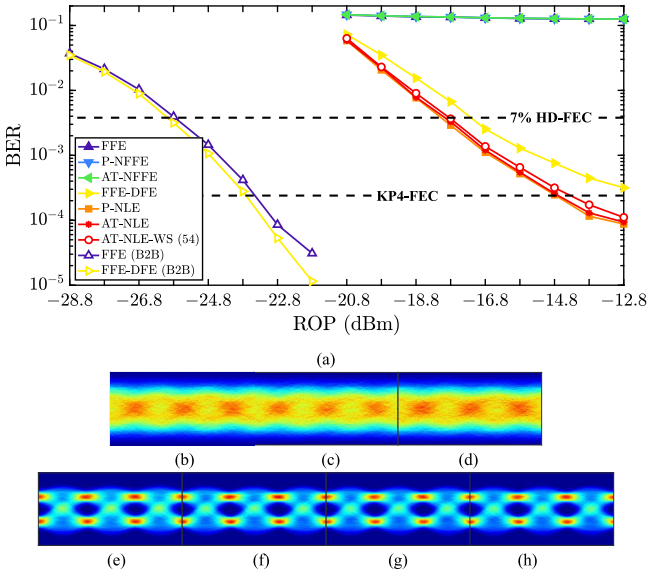

Fig. 7. (a) BER for 100-GBaud OOK transmission versus ROP under 100-km SSMF case using FFE, P-NFFE, AT-NFFE, FFE-DFE, P-NLE, AT-NLE, AT-NLE-WS, and under B2B case using FFE and FFE-DFE; (b-h): the corresponding recovered eye-diagrams under 100-km SSMF case at a ROP of −12.8 dBm.

- For P-NLE-WS, the RNRM is changed from 160 to 270 by varying the N_c from 10 to 120, clustering the estimated 470 weights from P-NLE with $N_1 = 170$, $N_2 = 150$, and $D_1 = 150$;
- For AT-NLE-WS, the RNRM is changed from 10 to 120 by varying the N_c from 10 to 120, clustering the estimated 470 weights from AT-NLE with $N_1 = 170$, $N_{AT} = 150$, and $D_1 = 150$.

To put it simply for Fig. 6, some key RNRM values are illustrated in Table 2. In regard to the complexity with the achieved BER under 7% HD-FEC BER limit of 3.8×10^{-3}, the FFE-DFE-WS with 14 multiplications at least outperforms others while AT-NLE-WS requires 16 multiplications at least. In this way, FFE-DFE-WS consumes only ~8.5% of RNRM of P-NLE-WS and <5% of RNRM of FFE-DFE, P-NLE, and AT-NLE. When BER reaches 2.4×10^{-4}, the KP4-FEC limit, the FFE-DFE and FFE-DFE-WS are unworkable. Meanwhile, the AT-NLE-WS still achieves the lowest RNRM of 28, greatly reducing 84.3%, 92.6%, and 93.6% of RNRM compared with the P-NLE-WS, AT-NLE, and P-NLE, respectively. Hence, among these equalizers, AT-NLE-WS is the optimal one in 100-Gb/s OOK transmission over a 100-km SSMF considering the complexity and BER performance.

What is more, the impact of ROP on BER performance for 54-cluster AT-NLE-WS, along with FFE, P-NFFE, AT-NFFE, FFE-DFE, P-NLE, and AT-NLE, is evaluated and results are shown in Fig. 7(a). The recovered eye-diagrams after equalization with them are presented in Fig. 7(b-h). Here all the equalizers are with parameters referring to the saturated BER performance at the maximal ROP of −12.8 dBm. One can see that all linear and nonlinear FFEs are inoperative. Compared with P-NLE and AT-NLE, achieving the best BER performance regardless of ROP, the AT-NLE-WS suffers the power penalties of about 0.4 dB and 0.2 dB with the achieved BER under KP4-FEC threshold and 7% HD-FEC threshold, respectively, while the FFE-DFE suffers the power penalty of about 1 dB at a BER of 3.8×10^{-3}. Still, AT-NLE-WS requires the lowest RNRM of 54 and has a small power penalty, in comparison with the P-NLE and AT-NLE requiring 620 and 470 real-valued multiplications, respectively. In addition, the BER results using FFE ($N_1 = 40$) and FFE-DFE ($N_1 = 40$ and $D_1 = 5$) under B2B are also depicted in Fig. 7(a) for comparison. Note that under B2B the memory lengths of $N_1 = 40$ and $D_1 = 5$ for FFE and FFE-DFE are enough to achieve the saturated BER performance at the measured ROPs and NFFEs do not improve the BER performance whose results are omitted here without distraction. Obviously, the power penalties between the 100-km transmission using P-NLE/AT-NLE(-WS) and B2B transmission using FFE/FFE-DFE are approximately 8 dB and 9 dB under the 7% HD-FEC limit and KP4-FEC limit, respectively. These penalties can be attributed to not only the SNR decrease of the optical signal but also the error propagation in DFE part of the P-NLE and AT-NLE.

3.2. 112-GBaud OOK results

The transmission data rate over a 100-km SSMF is further increased to 112 Gb/s, which is used to evaluate the superior performance of the AT-NLE-WS. In the same manner as in 100-Gb/s OOK transmission, the values of memory lengths N_1, N_2/N_{AT}, and D_1 for 112-Gb/s OOK transmission over a 100-km SSMF are firstly determined from the measured BER results at a ROP of −12.8 dBm, as shown in Fig. 8. The saturated BER of approximately 3×10^{-3} is achieved for FFE-DFE with $N_1 = 230$ and $D_1 = 170$, lower than the 7% HD-FEC limit showing the robustness of FFE-DFE combating CD in high-speed and long-distance transmissions. With nonlinear P-NLE and AT-NLE performed, the saturated BER can be further decreased to ~1.5×10^{-3} with $N_2/N_{AT} = 160$ but cannot reach the KP4-FEC threshold. Besides, the P-NLE and AT-NLE show the close BER performance similar as 100-Gb/s OOK transmission. Predictably, none of the FFE, P-NFFE, and AT-NFFE is operable in this 112-Gb/s OOK transmission over a 100-km SSMF.

Applied the parameters for FFE-DFE ($N_1 = 230$ and $D_1 = 170$), P-NLE ($N_1 = 230$, $N_2 = 160$, and $D_1 = 170$), AT-NLE ($N_1 = 230$, $N_{AT} = 160$, and $D_1 = 170$) at saturated BERs, the convergence curves of RLS using these equalizers are shown in Fig. 9. Similarly, 10,000 training symbols are sufficient for equalizers converging to achieve saturated BERs. Furthermore, the BER performance versus the number of clusters is evaluated for FFE-DFE-WS, P-NLE-WS, and AT-NLE-WS, as shown in Fig. 10 For all equalizers with weight-sharing, the close saturated BERs as those without weight-sharing can be achieved with 62 clusters for the P-NLE-WS and AT-NLE-WS, and 82 clusters for the FFE-DFE-WS.

The change of RNRM for FFE-DFE(-WS), P-NLE(-WS), and AT-NLE(-WS) is in the same fashion as in 100-Gb/s transmission but with different ranges. The resulting BERs are depicted in Fig. 11. All these performed equalizers can make the BERs below the BER of 3.8×10^{-3}. Key RNRM values are summarized in Table 3. In regard to the complexity with the achieved BER under the 7% HD-FEC BER limit, the AT-NLE-WS outperforms the other five equalizers, and reduces the RNRM by approximately 60%, 83.2%, 91.8%, 92.4%, and 92.7% compared with FFE-DFE-WS, P-NLE-WS, FFE-DFE, AT-NLE, and P-NLE, respectively. Thus, the AT-NLE-WS is still the optimal solution taking into account both the BER performance and computational complexity in 112-Gb/s OOK transmission over a 100-km SSMF.

Finally, the BER curves versus ROP using 62-cluster AT-NLE-WS and FFE, P-NFFE, AT-NFFE, FFE-DFE, P-NLE, and AT-NLE for 112-Gb/s OOK transmission over a 100-km SSMF are plotted in Fig. 12(a), in which all equalizers with the preset memory lengths/clusters satisfying the saturated BER performance at the maximal ROP of −12.8 dBm. The corresponding recovered eye-diagrams of these equalizers are presented

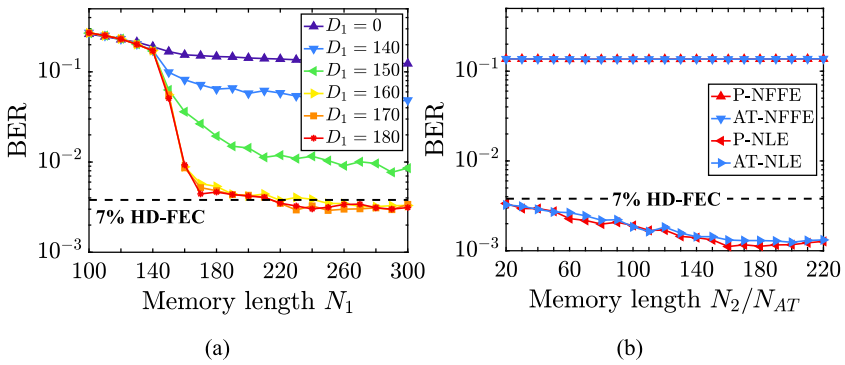

Fig. 8. (a) BER versus memory length of N_1 for FFE under different D_1 for DFE; (b) BER versus memory length of N_2/N_{AT} for FFE of P-NFFE/AT-NFFE ($N_1 = 230$ and $D_1 = 0$) and P-NLE/AT-NLE ($N_1 = 230$ and $D_1 = 170$), at a ROP of −12.8 dBm for 112-GBaud OOK transmission over a 100-km SSMF.

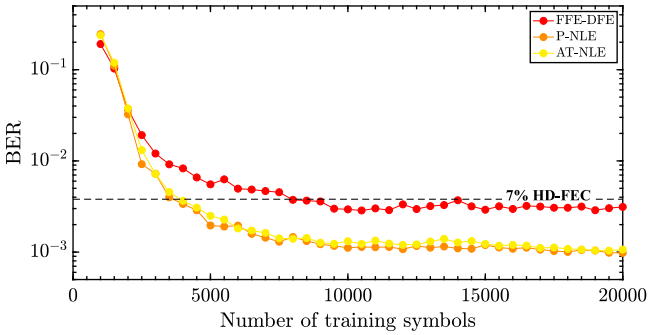

Fig. 9. BER versus the number of training symbols of 112-GBaud OOK signal transmission over a 100-km SSMF using different equalizers.

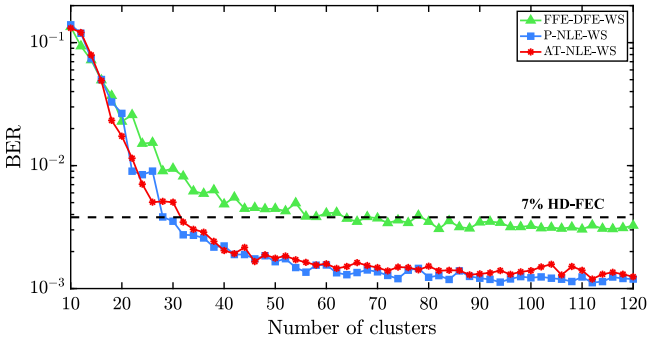

Fig. 10. BER versus the number of clusters for FFE-DFE-WS, P-NLE-WS, and AT-NLE-WS at a ROP of −12.8 dBm for 112-GBaud OOK transmission over a 100-km SSMF.

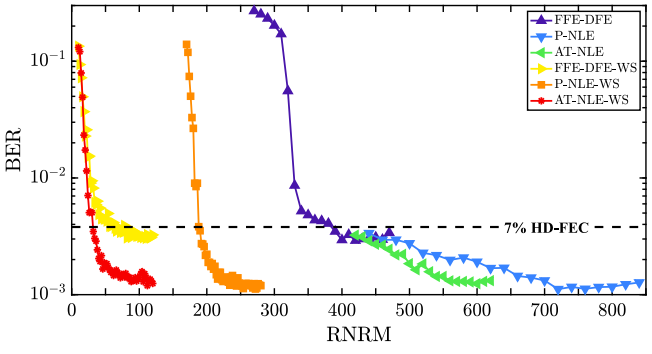

Fig. 11. BER versus RNRM using FFE-DFE, P-NLE, AT-NLE, FFE-DFE-WS, P-NLE-WS, and AT-NLE-WS at a ROP of −12.8 dBm for 112-GBaud OOK transmission over a 100-km SSMF.

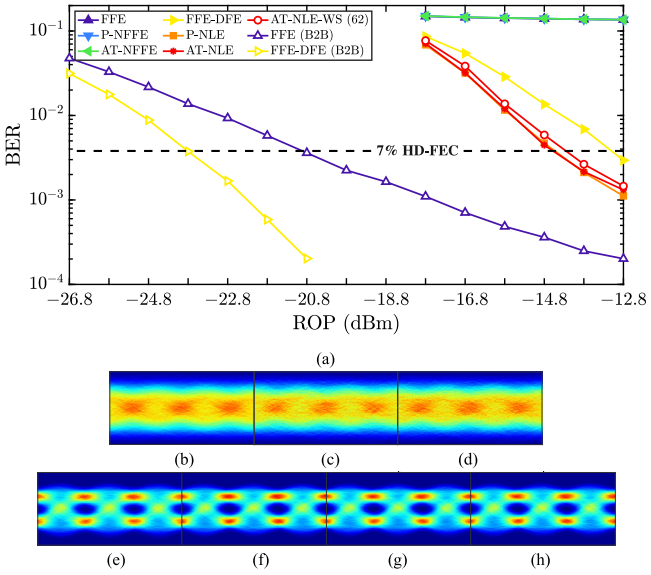

Fig. 12. (a) BER for 112-GBaud OOK transmission versus ROP under 100-km SSMF case using FFE, P-NFFE, AT-NFFE, FFE-DFE, P-NLE, AT-NLE, AT-NLE-WS, and under B2B case using FFE and FFE-DFE; (b-h): the corresponding recovered eye-diagrams under 100-km SSMF case at a ROP of −12.8 dBm.

Table 3
Key RNRMs [in Fig. 11] of all equalizers for 112-Gb/s OOK transmission over a 100-km SSMF.

Equalizer	RNRM at 3.8 × 10–3	RNRM at saturated BER
FFE-DFE	≥390	400
P-NLE	≥440	720
AT-NLE	≥420	560
FFE-DFE-WS	≥80	82
P-NLE-WS	≥190	222
AT-NLE-WS	≥32	62

in Fig. 12(b–h). It can be observed that the P-NLE and AT-NLE can achieve the best BER performance regardless of ROP. Compared with P-NLE and AT-NLE, 62-cluster AT-NLE-WS has the power penalty < 0.4 dB in terms of BER performance under the 7% HD-FEC limit at the benefit of RNRM decrease from 720 and 560 to 62, respectively. In addition, the B2B transmission of 112-Gb/s OOK using FFE ($N_1 = 40$) and FFE-DFE ($N_1 = 40$ and $D_1 = 5$) with saturated BER performance is compared and the corresponding results are also shown in Fig. 12. Different for FFE and FFE-DFE in 100-Gb/s B2B transmission with close BER performance at ROPs from −28.8 dBm to −21.8 dBm, the

power penalty of using them is increased to 3 dB owning to the more severe bandwidth limitation, under the 7% HD-FEC limit. As for the transmission power penalty, the value between 100-km transmission using P-NLE and AT-NLE(-WS) and B2B transmission using FFE is approximately 6 dB, while the value is enlarged to approximately 9 dB when B2B transmission using FFE-DFE. Compared with 8-dB power penalty in 100-Gb/s 100-km and B2B transmissions under 7% HD-FEC limit, this penalty is only enlarged by 1 dB in 112-Gb/s transmission.

4. Conclusion

In this paper, a comprehensive comparison among post-equalizers including FFE, P-NFFE, AT-NFFE, FFE-DFE, P-NLE, AT-NLE, FFE-DFE-WS, P-NLE-WS, and AT-NLE-WS has been conducted in terms of computational complexity and BER performance, in C-band 100-Gb/s/λ and 112-Gb/s/λ OOK transmission systems over a 100-km dispersion-uncompensated SSMF. The experimental results show that linear and nonlinear FFEs are powerless to combat large CD-induced frequency power fading and hence are inoperative in 100-km transmissions. After CD compensation using FFE-DFE(-WS), P-NLE(-WS), and AT-NLE(-WS), 100-Gb/s and 112-Gb/s data rates can be achieved for C-band 100-km transmissions. Thanks to absolute operation and weight sharing, the AT-NLE-WS not only achieves similar BER performance as other NLEs but also reduces the computational complexity by >80%. Although the hardware implementation of these algorithms has a long way to go, these low-cost algorithms pave the way for cost-efficient IM/DD transmissions in optical interconnections with single-wavelength data rate beyond 100 Gb/s and transmission distance up to 100 km. Especially for the AT-NLE-WS performed in 100-km SSMF transmissions, it shows satisfactory BER performance and considerably low complexity, requiring only 16 (28) real-valued multiplications for 100-Gb/s/λ OOK signal when the achieved BER reaching 7% HD-FEC (KP4-FEC) threshold, and 32 real-valued multiplications for 112-Gb/s/λ OOK signal when the achieved BER reaching 7% HD-FEC threshold.

Declaration of competing interest

The authors declare that they have no known competing financial interests or personal relationships that could have appeared to influence the work reported in this paper.

Data availability

Data will be made available on request.

Acknowledgments

This work was supported in part by the National Key R&D Program of China (No. 2018YFB1801701), in part by the National Natural Science Foundation of China (NSFC) (62101602, 62035018), and in part by the Hong Kong Government General Research Fund under project number PolyU 15220120 and PolyU 15217620.

References

[1] A. Mecozzi, C. Antonelli, M. Shtaif, Kramers–Kronig coherent receiver, Optica 3 (2016) 1220–1227, URL: http://opg.optica.org/optica/abstract.cfm?URI=optica-3-11-1220.

[2] D. Che, Q. Hu, W. Shieh, Linearization of direct detection optical channels using self-coherent subsystems, J. Lightwave Technol. 34 (2016) 516–524.

[3] D. Che, W. Shieh, Polarization demultiplexing for Stokes vector direct detection, J. Lightwave Technol. 34 (2016) 754–760.

[4] X. Chen, C. Antonelli, S. Chandrasekhar, G. Raybon, A. Mecozzi, M. Shtaif, P. Winzer, Kramers–Kronig receivers for 100-km datacenter interconnects, J. Lightwave Technol. 36 (2018) 79–89.

[5] C. Sun, T. Ji, H. Ji, Z. Xu, W. Shieh, Experimental demonstration of complex-valued DSB signal field recovery via direct detection, IEEE Photon. Technol. Lett. 32 (2020) 585–588.

[6] T. Ji, C. Sun, H. Ji, Z. Xu, Y. Peng, W. Shieh, Theoretical and experimental investigations of interleaved carrier-assisted differential detection, J. Lightwave Technol. 39 (2021) 122–128.

[7] H. Chen, H. Huang, N.K. Fontaine, R. Ryf, Phase retrieval with fast convergence employing parallel alternative projections and phase reset for coherent communications, Opt. Lett. 45 (2020) 1188–1191.

[8] H. Huang, H. Chen, Y. Huang, N.K. Fontaine, R. Ryf, Y. Song, Carrier-less phase retrieval receiver leveraging digital upsampling, Opt. Lett. 45 (2020) 6070–6073.

[9] H. Chen, N.K. Fontaine, M. Mazur, L. Dallachiesa, Y. Zhang, H. Huang, D. van Veen, V. Houtsma, A. Blanco-Redondo, R. Ryf, D.T. Neilson, 140G/70g direct detection PON with > 37 db power budget and 40-km reach enabled by colorless phase retrieval full field recovery, in: 2021 European Conference on Optical Communication, ECOC, 2021, pp. 1–4.

[10] H. Chen, N.K. Fontaine, R.-J. Essiambre, H. Huang, M. Mazur, R. Ryf, D.T. Neilson, Space-time diversity phase retrieval receiver, in: Optical Fiber Communication Conference (OFC) 2021, Optica Publishing Group, 2021, p. Th4D.3.

[11] R. Urata, H. Liu, X. Zhou, A. Vahdat, Datacenter interconnect and networking: from evolution to holistic revolution, in: Optical Fiber Communication Conference, Optica Publishing Group, 2017, p. W3G.1.

[12] X. Zhou, R. Urata, H. Liu, Beyond 1 tb/s IntraData center interconnect technology: IM-dd OR coherent? J. Lightwave Technol. 38 (2020) 475–484.

[13] C. Xie, J. Cheng, Coherent optics for data center networks, in: 2020 IEEE Photonics Society Summer Topicals Meeting Series, SUM, 2020, pp. 1–2.

[14] M. Zhu, J. Zhang, Q. Liu, B. Xu, X. Yi, Z. Yu, P. Zhang, K. Qiu, Experimental demonstration of 80-gb/s DSB ook signal transmission over 100-km SSMF with simplified Volterra based DFE, in: 26th Optoelectronics and Communications Conference, Optica Publishing Group, 2021, p. T2B.5.

[15] J. Li, Z. Wang, X. Li, Y. Su, Single-span IM/DD transmission over 120-km SMF with a silicon photonic mach–zehnder modulator and THP, in: Optical Fiber Communication Conference (OFC) 2022, Optica Publishing Group, 2022, p. M2H.3.

[16] S. Hu, J. Zhang, J. Tang, Q. Liu, W. Jin, Z. Zhong, R. Giddings, J. Zhou, T. Jin, X. Zhao, B. Xu, X. Gao, K. Qiu, 112-Gb/s PAM-4 IM/DD optical transmission over 100-km single mode fiber with linear equalizer, in: Optical Fiber Communication Conference (OFC) 2022, Optica Publishing Group, 2022, p. M2H.5.

[17] X. Wu, J. Zhang, A.P.T. Lau, C. Lu, C-band 120-gb/s PAM-4 transmissions over a 100-km dispersion-uncompensated SSMF using joint combined pulse shaping and low-complexity nonlinear equalization, Opt. Lett. 47 (2022) 5144–5147.

[18] R. Rath, D. Clausen, S. Ohlendorf, S. Pachnicke, W. Rosenkranz, Tomlinson–harashima precoding for dispersion uncompensated PAM-4 transmission with direct-detection, J. Lightwave Technol. 35 (2017) 3909–3917.

[19] Q. Hu, K. Schuh, M. Chagnon, F. Buchali, S.T. Le, H. Bulow, 50 Gb/s PAM-4 transmission over 80-km SSMF without dispersion compensation, in: 2018 European Conference on Optical Communication, ECOC, 2018, pp. 1–3.

[20] H. Xin, K. Zhang, D. Kong, Q. Zhuge, Y. Fu, S. Jia, W. Hu, H. Hu, Nonlinear tomlinson-harashima precoding for directdetected double sideband PAM-4 transmission without dispersion compensation, Opt. Express 27 (2019) 19156–19167.

[21] N.-P. Diamantopoulos, H. Nishi, W. Kobayashi, K. Takeda, T. Kakitsuka, S. Matsuo, On the complexity reduction of the second-order Volterra nonlinear equalizer for IM/DD systems, J. Lightwave Technol. 37 (2019) 1214–1224.

[22] Q. Zhang, S. Duan, Z. Wang, Y. Jiang, P. Li, B. Cao, Y. Wu, An improved Volterra nonlinear equalizer for 50 gb/s PAM4 IM/DD transmission with 10g-class optics, in: Asia Communications and Photonics Conference/International Conference on Information Photonics and Optical Communications 2020 (ACP/IPOC), Optica Publishing Group, 2020, p. S4H.7.

[23] Y. Yu, T. Bo, Y. Che, D. Kim, H. Kim, Low-complexity nonlinear equalizer based on absolute operation for C-band PAM signal generated by using directly modulated laser, in: 2020 OptoElectronics and Communications Conference, OECC, 2020, pp. 1–3.

[24] Y. Yu, M.R. Choi, T. Bo, Y. Che, D. Kim, H. Kim, Nonlinear equalizer based on absolute operation for IM/DD system using DML, IEEE Photon. Technol. Lett. 32 (2020) 426–429.

[25] Y. Yu, T. Bo, Y. Che, D. Kim, H. Kim, Low-complexity nonlinear equalizer based on absolute operation for C-band IM/DD systems, Opt. Express 28 (2020) 19617–19628.

[26] J. Zhang, Z. Lin, X. Wu, J. Liu, A.P.T. Lau, C. Guo, C. Lu, S. Yu, Low-complexity sparse absolute-term based nonlinear equalizer for C-band IM/DD systems, Opt. Express 29 (2021) 21891–21901.

[27] Q. Zhang, S. Duan, Z. Wang, B. Cao, Y. Wu, J. Chen, M. Wang, Low complexity Volterra nonlinear equalizer based on weight sharing for 50 gb/s PAM4 IM/DD transmission with 10g-class optics, Opt. Commun. 508 (2022) 127762.

[28] J. Zhang, T. Ye, X. Yi, C. Yu, K. Qiu, An efficient hybrid equalizer for 50 gb/s PAM-4 signal transmission over 50 km SSMF in a 10-GHz DML-based IM/DD system, in: 2017 Conference on Lasers and ElectroOptics, CLEO, 2017, pp. 1–2.

[29] X. Wu, J. Zhang, A.P.T. Lau, C. Lu, Low-complexity absolute-term based nonlinear equalizer with weight sharing for C-band 85-gbaud OOK transmission over a 100-km SSMF, Opt. Lett. 47 (2022) 1565–1568.

[30] J. Zhang, X. Wu, L. Sun, J. Liu, A.P.T. Lau, C. Guo, S. Yu, C. Lu, C-band 120-gb/s PAM-4 transmission over 50-km SSMF with improved weighted decision-feedback equalizer, Opt. Express 29 (2021) 41622–41633.
[31] X. Tang, Y. Qiao, Y.-W. Chen, Y. Lu, G.-K. Chang, Digital pre- and post-equalization for C-band 112-gb/s PAM4 short-reach transport systems, J. Lightwave Technol. 38 (2020) 4683–4690.
[32] X. Wu, J. Zhang, G. Zhou, A.P.T. Lau, C. Lu, C-band 112-gb/s PAM-4 transmission over 50-km SSMF using absolute-term based nonlinear FFE-dfe, in: Asia Communications and Photonics Conference 2021, Optica Publishing Group, 2021, p. M4I.3.
[33] X. Tang, S. Liu, X. Xu, J. Qi, M. Guo, J. Zhou, Y. Qiao, 50-Gb/s PAM4 over 50-km single mode fiber transmission using efficient equalization technique, in: Optical Fiber Communication Conference (OFC) 2019, Optica Publishing Group, 2019, p. W2A.45.
[34] J. Zhou, H. Wang, L. Liu, C. Yu, Y. Feng, S. Gao, W. Liu, Z. Li, C-band 56 gbit/s on/off keying system over a 100 km dispersion-uncompensated link using only receiver-side digital signal processing, Opt. Lett. 45 (2020) 758–761.
[35] H. Wang, J. Zhou, D. Guo, Y. Feng, W. Liu, C. Yu, Z. Li, Adaptive channel-matched detection for C-band 64-gbit/s optical OOK system over 100-km dispersion-uncompensated link, J. Lightwave Technol. 38 (2020) 5048–5055.
[36] Z. Chen, J. Nie, S. Zhang, Q. Yang, X. Dai, L. Deng, M. Cheng, D. Liu, 56-Gb/s/λ C-band DSB IM/DD PAM-4 40-km SSMF transmission employing a multiplier-free MLSE equalizer, Opt. Express 30 (2022) 11275–11287.
[37] C.-Y. Chuang, L.-C. Liu, C.-C. Wei, J.-J. Liu, L. Henrickson, W.-J. Huang, C.-L. Wang, Y.-K. Chen, J. Chen, Convolutional neural network based nonlinear classifier for 112-gbps high speed optical link, in: Optical Fiber Communication Conference, Optica Publishing Group, 2018, p. W2A.43.
[38] L. Yi, T. Liao, L. Huang, L. Xue, P. Li, W. Hu, Machine learning for 100 gb/s/λ passive optical net work, J. Lightwave Technol. 37 (2019) 1621–1630.
[39] J. Zhang, L. Yan, L. Jiang, A. Yi, Y. Pan, W. Pan, B. Luo, 56-Gbit/s PAM-4 optical signal transmission over 100-km SMF enabled by TCNN regression model, IEEE Photon. J. 13 (2021) 1–6.
[40] Z. Xu, C. Sun, J.H. Manton, W. Shieh, Joint equalization of linear and nonlinear impairments for PAM4 short-reach direct detection systems, IEEE Photon. Technol. Lett. 33 (2021) 425–428.
[41] Z. Xu, S. Dong, J.H. Manton, W. Shieh, Low-complexity multi-task learning aided neural networks for equalization in short-reach optical interconnects, J. Lightwave Technol. 40 (2022) 45–54.
[42] X. Wu, A.S. Karar, K. Zhong, A.P.T. Lau, C. Lu, Experimental demonstration of pre-electronic dispersion compensation in IM/DD systems using an iterative algorithm, Opt. Express 29 (2021) 24735–24749.
[43] M. Yin, D. Zou, W. Wang, F. Li, Z. Li, Transmission of a 56 gbit/s PAM4 signal with low-resolution DAC and pre-equalization only over 80 km fiber in C-band IM/DD systems for optical interconnects, Opt. Lett. 46 (2021) 5615–5618.
[44] G. Goeger, Applications of phase retrieval in high bit-rate direct-detection systems, in: Optical Fiber Communication Conference, Optica Publishing Group, 2016, p. Th2A.40.
[45] S. Hu, J. Zhang, J. Tang, T. Jin, W. Jin, Q. Liu, Z. Zhong, R. Giddings, Y. Hong, B. Xu, X. Yi, K. Qiu, Multi-constraint gerchberg–saxtoniteration algorithms for linearizing IM/DD transmission systems, Opt. Express 30 (2022) 10019–10031.
[46] R.W. Gerchberg, A practical algorithm for the determination of phase from image and diffraction plane pictures, Optik 35 (1972) 237–246.
[47] N. Aggarwal, K. Aggarwal, An Improved K-Means Clustering Algorithm for Data Mining, paperback, LAP LAMBERT Academic Publishing, 2012.
[48] J. Zhang, W. Chen, M. Gao, G. Shen, K-means-clustering-based fiber nonlinearity equalization techniques for 64-QAM coherent optical communication system, Opt. Express 25 (2017) 27570–27580.
[49] K. Zhong, X. Zhou, J. Huo, C. Yu, C. Lu, A.P.T. Lau, Digital signal processing for short-reach optical communications: A review of current technologies and future trends, J. Lightwave Technol. 36 (2018) 377–400.
[50] H. Zhou, Y. Li, Y. Liu, L. Yue, C. Gao, W. Li, J. Qiu, H. Guo, X. Hong, Y. Zuo, J. Wu, Recent advances in equalization technologies for short-reach optical links based on PAM4 modulation: A review, Appl. Sci. 9 (2019).
[51] A. Zaknich, Principles of Adaptive Filters and Self-Learning Systems, Springer Science & Business Media, 2005.
[52] J.G. Proakis, M. Salehi, Digital Communications, Volume 4, McGraw-hill New York, 2001.